Innovative L-band electron paramagnetic resonance investigation of solid-state pouch cell batteries

Charles-E Dutoit[1,2], Raffaella Soleti[3,4], Jean-Marie Doux[5], Vincent Pelé[5], Véronique Boireau[5], Christian Jordy[5], Simon Pondaven[2,6], and Hervé Vezin[1,2]

[1] Université Lille Nord de France, CNRS, UMR8516, LASIRE, 59655 Villeneuve d'Ascq, France
[2] Centre de Résonance Magnétique Electronique pour les Matériaux et l'Energie, 59655 Villeneuve d'Ascq, France
[3] Université d'Angers, Inserm UMR1307, CNRS UMR6075, Nantes Université, CRCI2NA, F-49000 Angers, France
[4] Université d'Angers, SFR ICAT, Plateforme RPE, F-49000 Angers, France
[5] SAFT, Direction de la Recherche, 111 Boulevard Alfred Daney, 33074 Bordeaux, France
[6] TotalEnergies OneTech R&D, Centre de Recherche de Solaize (CRES), chemin du canal, BP 22, 69360 Solaize, France

Correspondence: Charles-E Dutoit (charles.dutoit@univ-lille.fr)

Abstract. Usually, the conventional electron paramagnetic resonance (EPR) spectroscopy and imaging use a microwave cavity operating at X-band, i.e. with an excitation frequency of around 9.6 GHz, and remains the most popular mode in the magnetic characterization of lithium batteries to date. We provide here the first low-frequency EPR investigations for monitoring the metallic lithium structures in the solid-state pouch cell batteries. We show that L-band, i.e. a microwave frequency of around 1.01 GHz, is an invaluable method to probe in depth the electrode components through a standard pouch cell using aluminum laminated film for packaging without opening the battery. These results offer a new approach for monitoring the nucleation of micrometric and sub-micrometric lithium particles such as dendritic lithium structures which is an important step in the development of reliable solid-state batteries.

1 Introduction

Lithium-ion batteries offer high energy densities making them appealing for a wide range of applications. Conventional Li-ion cells are composed of a Li-containing oxide as a positive electrode material and graphite as a negative electrode material. The Li^+ ionic transfer between the electrodes is done through a liquid electrolyte flooding both electrodes and a separator keeping both electrodes apart (Armand and Tarascon, 2008). One of the attractive cathodes for commercial use is made up of a lithium containing metal oxide such as lithium, nickel, manganese, cobalt, oxide commonly known as NMC (Santhanam and Rambabu, 2009; Yaqub et al., 2014; Leng et al., 2017). These elements form a stable structure to hold the lithium-ions when the battery is in a discharged state. With the goal of improving the energy density and safety of cells, the replacement of the liquid electrolyte by a solid compound (gel, polymer, ceramic or their combination) is being studied in solid-state batteries (Agrawal and Pandey, 2008; Hatzell et al., 2020). While most commercial Li-ion cells are hosted in rigid structures (cylindrical and prismatic cells), softer casing made of laminated aluminum and polymer layer are also being developed for the pouch cell packaging. This format can easily be made into different shapes and sizes while benefiting from a lightweight packaging which is a serious advantage for mobility applications. Owing to a lightweight aluminum packaging, pouch cells can be used in small portable

electronics such as drones, mobile and so one. Compared to rigid cylindrical cells, they offer a good weight to energy ratio. Considering the versatility of the pouch cell format, it is also adapted for the solid-state battery. Furthermore, the packaging is not a rigid enclosure and a special attention is needed because of safety concerns during short-circuits or overcharge events as the pressure buildup can cause cell swelling (Chen et al., 2021). Such short-circuits, usually caused by the nucleation of metallic lithium aggregates during lithiation processes can pose a serious risk of explosion. Early non-destructive detection of lithium growth is mandatory to avoid such risk in this cell format. In this work, using continuous-wave L-band electron paramagnetic resonance (cw-EPR) spectroscopy and imaging, we report, for the first time, the possibility of analyzing the metallic lithium structures in the solid-state pouch cell batteries directly through the standard aluminum laminated film. One of limitations in the EPR characterization of an electrochemical cell is the cell design which have to be compatible with the standard resonator dimension. In previous EPR measurements, we designed a millimetric cylindrical electrochemical cell specially adapted for X-band spectrometers (Salager et al., 2014; Sathiya et al., 2015; Dutoit et al., 2021). It should be noted that all previous in situ EPR results bave been performed on electrochemical cell models using a Kapton film, PET/EVA film or other types of EPR silent polymers which are not a standard packaging for batteries (Geng et al., 2021). Herein, we demonstrate that the electrode materials enveloped in an Al-based pouch film used as a standard packaging materials for batteries (Park et al., 2021) can be characterized without opening the battery. This result offers a new approach paving the way for operando characterization of commercial pouch cell batteries.

2 Experimental details

2.1 Samples

Two types of cells were assembled using the same positive electrode and separator layers with either a Li-metal or Si-based negative electrode. An argyrodite-type sulfide electrolyte was selected as the solid electrolyte (SE: Li_6PS_5Cl from NEI corporation). The positive electrode, separator and Si-based negative electrode were all prepared using a wet process using isobutyl isobutylene and xylene solvents with PVdF-based copolymer as binders for the electrodes and an in-house specific binder for the separator. All the materials were handled and processed in Ar-filled glove box. For the positive electrode, NMC811 ($LiNi_{0.8}Mn_{0.1}Co_{0.1}O_2$, commonly used by cathode) and SE powders were dispersed in a binder gel solution using a planetary mixer. A slurry containing NMC811, SE and PVdF was casted on a carbon-coated Al foil with a doctor blade with a 20.5 mg/cm^2 loading. For the Si-based negative electrode, Si (μm size), SE and Super P carbon were dispersed in the binder gel solution. A slurrry containing Si, SE, C and PVdF was casted on a carbon-coated Cu foil with a doctor blade and a 2.9 mg/cm^2 loading was obtained. For the separator, the SE powder was dispersed in the binder gel solution; and the obtained SE:binder (weight ratio 97:3) slurry was casted on a release-type PET film with a doctor blade. All the layers were dried at room temperature in the glove box. The uncalendared separator had a thickness of 130 μm ($\pm$10 μm) and could be peeled off from the PET film to recover a self-standing solid electrolyte layer. The Li metal had a thickness of 60 μm. The different layers were punched. The positive and negative electrodes were welded to tabs and set in the PP-coated aluminum laminated, before sealing the obtained pouch. The pouch, made of aluminum laminated (120 μm) containing one polyamide layer and

one polypropylene layer, was compacted under 300 MPa using a cold isostatic press to densify the layers and improve the electrode/separator contacts. The voltage was then controlled with a voltmeter and it was checked that the voltage was above 2 V indicating that ~~to ensure~~ the pouchs were not short-circuited.

2.2 Electron paramagnetic resonance spectroscopy

Continuous wave (cw) EPR experiments were performed using an L-band Bruker spectrometer operating at microwave frequency of around 1.01Ghz. EPR measurements were made at room temperature in a cylindrical microwave loop-gap cavity produced by Bruker (L-band BLGR 36mm E1978). The microwave power applied into the loop-gap cavity was set to 36 mW. The modulation amplitude of the magnetic field was taken at 0.3 mT. Other spectrometer settings were: sweep width, ~~200 G~~20 mT; conversion time, 40 ms; number of scans, 1; sweep time, 40.96 s. Simulations were done using the EasySpin package for MATLAB (Stoll and Schweiger, 2006).

2.3 Electron paramagnetic resonance imaging

EPRI measurements were performed with an L-band Bruker imaging spectrometer equipped with a three-axes gradient coil set with gradients along the x-axis (perpendicular to $\mathbf{Y}$ and $\mathbf{H}_0$), y-axis (perpendicular to $\mathbf{X}$ and $\mathbf{H}_0$) and z-axis (along $\mathbf{H}_0$). Images were done with a gradient strength of ~~42 G/cm~~4.2 mT/cm and a field-of-view of 30 mm. A total of 157 projections were recorded for each image. The high resolution images were reconstructed with a size of ~~512x512~~200x200 pixels which gives a pixel size of 150 μm. The recorded projections under gradient were deconvoluted from a signal obtained without gradient. Finally, the spatial-spatial images were obtained after a filtered back-projection.

3 Results and Discussion

Low frequency EPR experiments were carried out to probe electrode materials of two solid-state pouch cell batteries. In situ pouch cells were measured at the pristine state without opening the batteries. Figure 1 shows the real dimensions of the NMC‖Li^0 pouch cell battery and its orientation inside the loop-gap cavity. Usually, $\mathbf{Z}$ axis corresponds to the static magnetic field direction ($\mathbf{B}$). The pouch cells, 65x38 mm, are placed in the microwave loop-gap cavity (diameter, $\sim$40 mm; length, $\sim$70 mm) such as the battery plane is oriented along the static magnetic field, i.e. perpendicular to the $\mathbf{Y}$ axis. However, probing conduction electrons in metallic structures is not trivial due to a limited penetration of the microwave in the conductor also known as the skin depth. Indeed, it is well known that EPR line shape of metallic conductors is sensitive to the metal-thickness and the skin depth. In an EPR experiment, the electromagnetic field penetrates only the skin depth δ_{mw} and only the spins located in this area are ~~irradiated~~ excited. Consequently, the line shape is influenced by the homogeneous of the electromagnetic field in the metallic structure displaying a Dysonian line shape when a fraction of the electronic spins experiencing the microwave field and a pure Lorentzian in the opposite case for which all the electronic spins are excited. ~~Furthermore, this phenomenon depends on the spin coherent time T$_2$, in which electron travels on a specific distance δ_e, named spin depth. In metallic lithium structures, T$_2 \sim 10^{-9}$ s~~ $T_2 \sim 10^{-8}$ s ~~and then when.~~ When the metal thickness is much higher than the skin
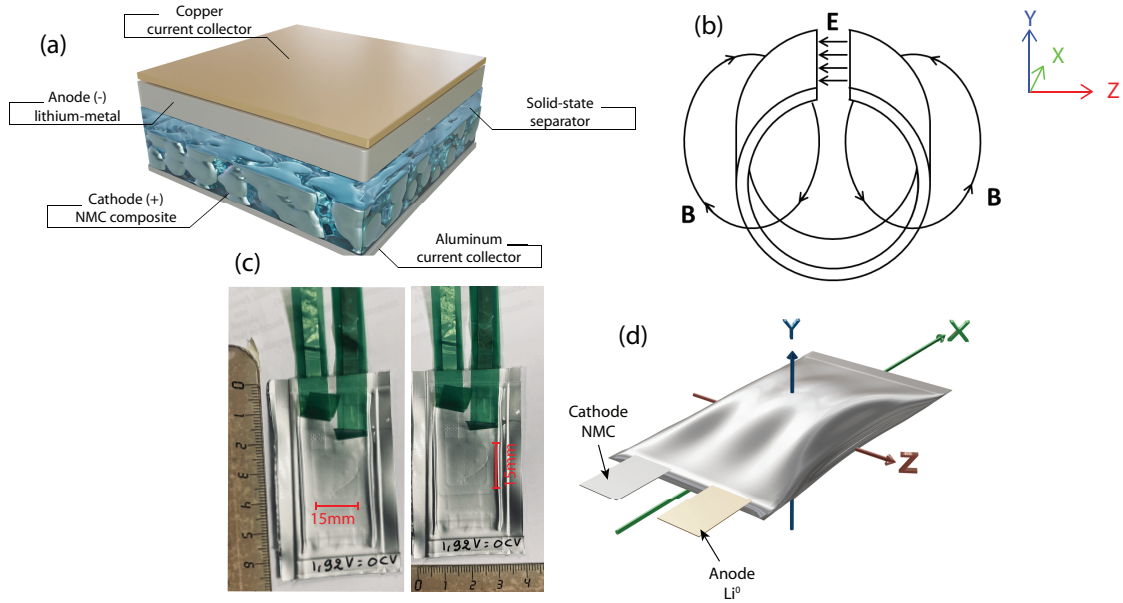
Figure 1. Examples of pouch cells studied in this work. (a) Schematic representation of the stacking used in our solid-state battery NMC‖Li^0. (b) Sketch of a microwave loop-gap cavity used for L-band EPR spectroscopy. The electrical field (**E**) is confined to the capacitive gap whereas the magnetic field (**B**) is confined inside the inductive loop. (c) Digital photos of the NMC‖Li^0 pouch cell. (d) Schematic representation of the pouch cell with its orientation inside the microwave loop-gap cavity.

depth, the EPR spectrum exhibits an asymmetric (Dysonian) line shape characterized by the ratio A/B ≫1 resulting from the apparent amplitude ratio between its positive lobe and negative lobe (Gourier et al., 1989; Niemöller et al., 2018; Dutoit et al., 2021). This skin depth can be easily calculated from the equation defined by:

$$\delta_{mw} \propto \sqrt{\frac{\rho}{f}} \tag{1}$$

90   where ρ is the metallic resistivity and f is the microwave frequency applied inside the cavity. It can be seen that the skin depth is proportional to $1/\sqrt{f}$. However, the physical size and the conductive behavior of the standard laminated aluminum packaging lead an additional challenge for monitoring electrode materials. Indeed, placing a large metallic conductor inside a standard X-band microwave cavity can cause serious perturbations of the dielectric making it impossible to tune the cavity. Nevertheless, getting an optimal tuning is essential to perform EPR measurements. Consequently, we turned to L-band EPR

95   spectroscopy and imaging which have a large loop-gap cavity adapted for standard solid-state pouch cell batteries, i.e. without specific battery preparation needed for X-band. In a such loop-gap cavity, the electrical field **E** is confined to the capacitive gap and the magnetic field **B** inside the inductive loop. As a result, the dielectric is slightly perturbed by inserting the metallic

sample (see Figure 1(b)). Furthermore, at L-band, the skin depth increases compared to X-band giving a better microwave penetration through the metallic body ($\sim$3 μm for aluminum at 1 GHz).

100   Figure 2(a) gives the L-band EPR spectrum of the NMC$\|$Li^0 pouch cell recorded at room temperature and in continuous wave through the standard aluminum laminated packaging. This signal exhibits a Dysonian line shape usually found for conduction electrons (Dyson, 1955; Feher and Kip, 1955). To obtain more information about the nature of this metallic complexes like the g-factor and the linewidth, we have simulated the spectrum with a phase shifted Lorentzian function, i.e. a sum of Lorentzian shaped absorption and dispersion functions, modeling the Dysonian shape (Gourier et al., 1989; Wandt et al., 2015). It can

105   be seen that the EPR spectrum is characterized by: (i) a single line centered at a g-factor of around 2.004 ± 2.10^{-3}, (ii) a peak-to-peak linewidth of 0.3 mT, (iii) an asymmetric ratio A/B around 3.7, as expected for metallic lithium structures. It is worth noting that the skin depth is around 4 μm for Li^0 complexes at 1 Ghz. This result indicate that the metallic structure size detected is much higher than 4 μm consistent with the metallic electrode dimensions. As the solid-state NMC$\|$Li^0 battery is composed of a metallic lithium electrode, we may compare the spectral signature relative to a non-metallic battery taken

110   as reference. The result is given in Figure 2(b) where lithium metal anode is replaced by Si-based electrode. As expected, initially the solid-state NMC$\|$Si-based battery, which contains Li$^+$ (EPR silent), Ni^{2+} (S=1), Ni^{3+} (S=1/2), Mn^{4+} (S=3/2), Co^{3+} (diamagnetic) and O^{2-} (EPR silent), gives no metallic lithium spectrum at the pristine state. However, as reported in the literature (Tang et al., 2017) , at room temperature NMC material exhibits an EPR signal centered at a g-value of around 2.00 with a linewidth of around 22 mT arising from Mn^{4+}, Ni^{2+} and Ni^{3+} ~~ions. The presence of Ni^{2+} and Ni^{3+} in the NMC sample~~

115   ~~is known to create an additional spectral broadening of the Mn^{4+} peak.~~ The manifestation of the ~~Mn^{4+}~~NMC is represented by a distortion of the baseline. This distortion is clearly visible ~~for~~ in the NMC$\|$Si-based cell but invisible ~~for~~ in the NMC$\|$Li^0 cell due to the intense Li^0 signal. Nevertheless, a single EPR peak is observed, displaying a g-factor near the free electron g-value (g_e=2.0023), originates from SiO$_2$ defects of the anode.
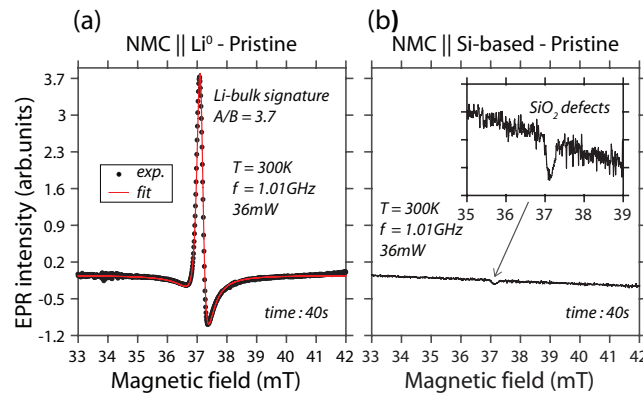

Figure 2. Continuous wave L-band EPR spectra of two solid-state batteries recorded through the aluminum laminated pouch cell at room temperature and at the pristine state: (a) NMC$\|$Li^0; (b) NMC$\|$Si-based battery. Modulation amplitude = 0.3 mT. Microwave power = 36 mW. Microwave frequency = 1.01 GHz
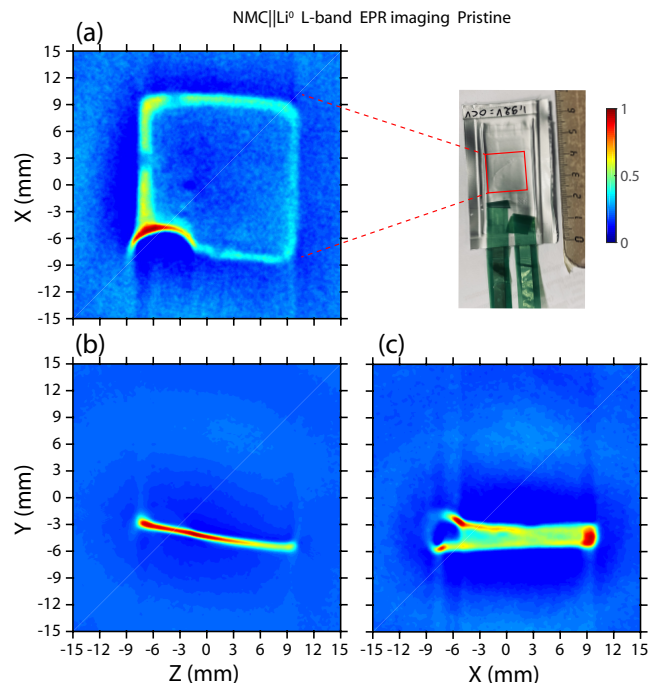
Figure 3. In situ L-band EPR imaging of a solid-state pouch cell NMC∥Li^0 battery recorded using the spatial-spatial detection scheme and in the XZ plane (a), YZ plane (b) and YX plane (c) respectively.

In order to verify that the metallic lithium spectrum does not originate from an impurity inside the pouch cell, we turned to the spatial-spatial imaging of the NMC∥Li^0 solid state battery to localize the anode part. As we saw previously, metallic lithium structures give a relatively sharp spectrum with a linewidth of around ~~3 G (with 0.1 mT = 1 G)~~0.3 mT. Using a gradient strength of ~~42 G/cm^2~~4.2 mT/cm^2 and thanks to the sharp line of Li^0, high resolution EPR images in the spatial planes XZ, YZ and YX respectively are expected. After placing the pouch cell directly in the center of the microwave loop-gap cavity and gradient coils, we recorded each image at room temperature. The time needed for each spatial-spatial image is around 60 min with a pixel size of 150 μm and a field-of-view of 30 mm. Figure 3 presents the EPR images for a NMC∥Li^0 solid-state pouch cell battery. For more clarity, we chose to reconstruct the spin concentration using a contour map with the red contour for the highest amplitude and the blue contour for the lowest amplitude. Contrary to recent investigations using the X-band EPR imaging to monitoring electrochemical batterie and for which the packaging was made with a non-standard material, such as a a Kapton film (Geng et al., 2021; Kang et al., 2024), the L-band image contains the spin distribution of electrode materials directly through the standard aluminum laminated pouch cell. The Li^0 anode part of the pouch cell is clearly visible and appears with a square shape (15 mmx15 mm) in the center of image. In the limit of the resolution of an L-band EPR spectrometer, this shape and its dimension are similar to the real size of the anode. However, a ~~slight~~ variation of the EPR intensities is observed between the edge and the middle of the anode. As shown by Niemöller and coworkers, the EPR signal of the thick and flat metallic electrode

(much thicker than the skin depth) gives a higher apparent intensity at the edge which hides the weaker signal in the middle part of the lithium foil. The physical origin of this contrast, characterized by extreme sensitivity of the edge to the microwave field, comes from a local variation of the microwave field caused by shielding and/or Eddy current effects (Niemöller et al., 2018). Nevertheless, in the case of sub-micrometric Li-metal nucleation, such as mossy/ dendritic lithium, this contrast will not be observed owing to the small size of such particles for which the electromagnetic field penetrates the whole metal. As reported in the literature, during electrochemical cycling, an intense and symmetric EPR spectrum can appears. This feature is the manifestation of an alteration of the metallic anode surface which creates sub-micrometric lithium aggregates. However, in the present work, we did not perform operando measurements and we did not observe an EPR signature of sub-micrometric lithium aggregates. Furthermore, in Figure 3(a), an intense curved shape localized at X=-6 mm and Z=-6 mm corresponding to the highest amplitude can be observed. This result indicates a local defect much more sensitive to the microwave field which corresponds to the interface between the lithium electrode and the copper current collector. Finally, images in the YZ and YX planes provide evidence that battery alignment inside the microwave loop-gap cavity is essential to reduce errors and misinterpretations. It can be seen that our solid-state pouch cell is slightly tilted in the loop-gap, which may also explain the apparent amplitude variation. Nevertheless, a three-axis field gradient associated with an L-band EPR spectrometer will enable us to locate metallic lithium structures through a standard packaging for batteries with a better spatial accuracy and then will improve the knowledge of Li-metal nucleation processes.

4 Conclusions

In conclusion, NMC‖Li^0 and NMC‖Si-based solid-state pouch cell batteries have been studied by continuous-wave (cw) L-band EPR spectroscopy and imaging. We provide first evidence of EPR characterization for pouch cell batteries using a standard aluminum laminated packaging. We observed a metallic lithium EPR spectrum and a SiO_2 defects signal through the aluminum laminated film. An advantage of conventional cw-EPR spectroscopy at L-band is that a centimeter size pouch cell using an aluminum laminated film material can be analyzed without preparation, without using a home-made cell specially designed for EPR and without opening the electrochemical battery.

For future studies, an operando EPR analysis of standard pouch cell batteries for solid-state or Li-ions technologies will provide additional information about the degradation processes and Red/ox evolution by probing electrode materials directly through a standard aluminum laminated film forming the pouch cell. We think our new approach would provide valuable insight for the battery community in terms of formulation, optimization and quality control of standard and commercial batteries.

Code availability. Matlab is a commercial software from MatlabWorks and the Easyspin package is available from https://easyspin.org/

Data availability. The dataset that support the findings of this investigation is available here: https://doi.org/10.5281/zenodo.14034164.

References

175   Agrawal, R. C. and Pandey, G. P.: Solid polymer electrolytes: Materials designing and all-solid-state battery applications: An overview, Journal of Physics D: Applied Physics, 41, https://doi.org/10.1088/0022-3727/41/22/223001, 2008.

Armand, M. and Tarascon, J.: Building better batteries, Nature, 451, 2–7, 2008.

Chen, Y., Kang, Y., Zhao, Y., Wang, L., Liu, J., Li, Y., Liang, Z., He, X., Li, X., Tavajohi, N., and Li, B.: A review of lithium-ion battery safety concerns: The issues, strategies, and testing standards, Journal of Energy Chemistry, 59, 83–99,
180   https://doi.org/10.1016/j.jechem.2020.10.017, 2021.

Dutoit, C. E., Tang, M., Gourier, D., Tarascon, J. M., Vezin, H., and Salager, E.: Monitoring metallic sub-micrometric lithium structures in Li-ion batteries by in situ electron paramagnetic resonance correlated spectroscopy and imaging, Nature Communications, 12, 1–6, https://doi.org/10.1038/s41467-021-21598-2, 2021.

Dyson, F. J.: Electron spin resonance absorption in metals. I. Experimental, Phys. Rev., 98, 349–359, 1955.

185   Feher, G. and Kip, A. F.: Electron Spin Resonance Absorption in Metals. I. Experimental, Physical Review B, 98, 337–348, 1955.

Geng, F., Yang, Q., Li, C., Hu, B., Zhao, C., Shen, M., and Hu, B.: Operando EPR and EPR Imaging Study on a NaCrO2 Cathode: Electronic Property and Structural Degradation with Cr Dissolution, The Journal of Physical Chemistry Letters, 12, 781–786, https://doi.org/10.1021/acs.jpclett.0c03327, pMID: 33410689, 2021.

Gourier, D., Barret, J. P., and Vivien, D.: Electrochemical stability of β-alumina and NASICON: ESR characterization of large metallic
190   sodium precipitates, Solid State Ionics, 31, 301–311, https://doi.org/10.1016/0167-2738(89)90470-0, 1989.

Hatzell, K. B., Chen, X. C., Cobb, C. L., Dasgupta, N. P., Dixit, M. B., Marbella, L. E., McDowell, M. T., Mukherjee, P. P., Verma, A., Viswanathan, V., Westover, A. S., and Zeier, W. G.: Challenges in Lithium Metal Anodes for Solid-State Batteries, ACS Energy Letters, 5, 922–934, https://doi.org/10.1021/acsenergylett.9b02668, 2020.

Kang, S., Geng, F., Li, Z., Jiang, Y., Shen, M., Chen, Q., Lou, X., and Hu, B.: Progressive Self-Leveling Deposition Improves the Cyclability
195   of Anode-less Sodium Metal Batteries Revealed by In Situ EPR Imaging, ACS Energy Letters, 9, 1633–1638, 2024.

Leng, Y., Ge, S., Marple, D., Yang, X.-G., Bauer, C., Lamp, P., and Wang, C.-Y.: Electrochemical Cycle-Life Characterization of High Energy Lithium-Ion Cells with Thick Li(Ni$_{0.6}$Mn$_{0.2}$Co$_{0.2}$)O$_2$ and Graphite Electrodes , Journal of The Electrochemical Society, 164, A1037–A1049, https://doi.org/10.1149/2.0451706jes, 2017.

Niemöller, A., Jakes, P., Eichel, R. A., and Granwehr, J.: EPR Imaging of Metallic Lithium and its Application to Dendrite Localisation in
200   Battery Separators, Scientific Reports, 8, 1–7, https://doi.org/10.1038/s41598-018-32112-y, 2018.

Park, B. K., Jeong, Y. K., Yang, S. Y., Kwon, S., Yang, J. H., Kim, Y. M., and Kim, K. J.: Deterioration behavior of aluminum pouch film used as packaging materials for pouch-type lithium-ion batteries, Journal of Power Sources, 506, 230 222, https://doi.org/10.1016/j.jpowsour.2021.230222, 2021.

Salager, E., Sarou-Kanian, V., Sathiya, M., Tang, M., Leriche, J.-b., Melin, P., Wang, Z., Vezin, H., Bassada, C., Deschamps, M., and
205   Tarascon, J.-M.: Solid-State NMR of the Family of Positive Electrode Materials Li$_2$Ru$_{1-y}$Sn$_y$O$_3$ for Lithium-Ion Batteries, Chemistry of Materials, 26, 7009–7019, https://doi.org/10.1021/cm503280s, 2014.

Santhanam, R. and Rambabu, B.: Improved high rate cycling of Li-rich Li$_{1.10}$Ni$_{1/3}$Co$_{1/3}$Mn$_{1/3}$O$_2$ cathode for lithium batteries, International Journal of Electrochemical Science, pp. 1770–1778, https://doi.org/10.1149/2.0451706jes, 2009.

Sathiya, M., Leriche, J. B., Salager, E., Gourier, D., Tarascon, J. M., and Vezin, H.: Electron paramagnetic resonance imaging for real-time
210   monitoring of Li-ion batteries, Nature Communications, 6, 1–7, https://doi.org/10.1038/ncomms7276, 2015.

Stoll, S. and Schweiger, A.: EasySpin, a comprehensive software package for spectral simulation and analysis in EPR, Journal of Magnetic Resonance, 178, 42–55, https://doi.org/10.1016/j.jmr.2005.08.013, 2006.

Tang, M., Dalzini, A., Li, X., Feng, X., Chien, P. H., Song, L., and Hu, Y. Y.: Operando EPR for Simultaneous Monitoring of Anionic and Cationic Redox Processes in Li-Rich Metal Oxide Cathodes, Journal of Physical Chemistry Letters, 8, 4009–4016, https://doi.org/10.1021/acs.jpclett.7b01425, 2017.

Wandt, J., Marino, C., Gasteiger, H. A., Jakes, P., Eichel, R.-A., and Granwehr, J.: Operando electron paramagnetic resonance spectroscopy – formation of mossy lithium on lithium anodes during charge–discharge cycling, Energy Environ. Sci., 8, 1358–1367, https://doi.org/10.1039/C4EE02730B, 2015.

Yaqub, A., Lee, Y. J., Hwang, M. J., Pervez, S. A., Farooq, U., Choi, J. H., Kim, D., Choi, H. Y., Cho, S. B., and Doh, C. H.: Low temperature performance of graphite and $LiNi_{0.6}Co_{0.2}Mn_{0.2}O_2$ electrodes in Li-ion batteries, Journal of Materials Science, 49, 7707–7714, https://doi.org/10.1007/s10853-014-8479-6, 2014.